Journal of Materials Chemistry A

Accepted Manuscript

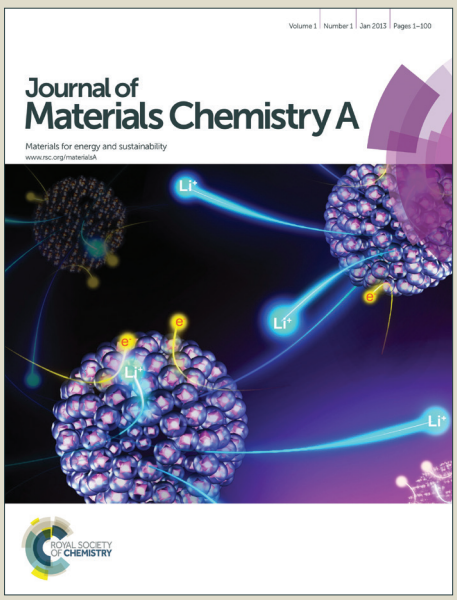

ROYAL SOCIETY OF CHEMISTRY

www.rsc.org/materialsA

Journal Name

COMMUNICATION

Facile synthesis of one-dimensional $LiNi_{0.8}Co_{0.15}Al_{0.05}O_2$ microrods as advanced cathode materials for lithium ion batteries

Received 00th January 20xx,
Accepted 00th January 20xx

DOI: 10.1039/x0xx00000x

www.rsc.org/

Naiteng Wu,[a] Hao Wu,[a,*] Wei Yuan,[a] Shengjie Liu,[a] Jinyu Liao[a] and Yun Zhang[a,*]

One-dimensional $LiNi_{0.8}Co_{0.15}Al_{0.05}O_2$ microrods are synthesized through chemical lithiation of mixed Ni, Co, and Al oxalate microrods obtained *via* a two-step co-precipitation strategy. The rod-like morphology together with high structural stability endows the $LiNi_{0.8}Co_{0.15}Al_{0.05}O_2$ microrods with superior rate capability and cycling performance for highly reversible lithium storage.

Nowadays, growing efforts are being devoted to developing advanced lithium-ion batteries (LIBs) for electric vehicles (EVs) and plug-in hybrid vehicles (PHEVs) due to global environmental concerns.[1] The desired cathode materials with high energy density and superior thermal stability play a critical role in the development of the next generation of LIBs.[2] $LiNiO_2$ is deemed as an alternative cathode material to currently commercialized $LiCoO_2$, due to its layered structure, high capacity, low cost, and low toxicity.[3,4] However, it still remains great challenges to synthesize high performance $LiNiO_2$ cathode materials because delithiated $LiNiO_2$ at elevated temperatures favors the generation of Ni^{2+} instead of Ni^{3+} and results in numerous Ni^{2+}-occupied sites in the Li layer,[5-7] thus giving rise to low Li^+-ion conductivity and poor electrochemical properties.

In order to overcome these obstacles, there have been extensive research efforts devoted to introducing other metal ions (e.g. Co, Mn, Al) into $LiNiO_2$ for partial substitution at the Ni site.[8,9] In particular, Co and Al co-substitution has been a substantial way to ameliorate the electrochemical behaviors of $LiNiO_2$, not only because Co substitution is able to improve the structural stability and the reversibility of delithiated $LiNiO_2$,[10] but also because additional substitution of Al into the lattice structure helps to stabilize the layered structure of $LiNiO_2$ as well as enhances its thermal stability.[11,12] Among the various Ni-based layered oxides in the form of $LiNi_{1-x-y}Co_xAl_yO_2$ (conventionally referred to as NCA), $LiNi_{0.8}Co_{0.15}Al_{0.05}O_2$, being successfully adopted in commercial LIBs, has been considered as a promising cathode material for EV applications, due to its high discharge capacity (~200 mAh/g), good structural stability, and low cost.[13] Nevertheless, this material easily undergoes a drastic power fading at high discharge/charge rates and/or at elevated temperatures,[14] due to the increased impedance and thermal instability of NCA,[15] thereby hampering the scalable application of NCA in EV and PHEV systems.

Cation doping[16,17] and surface coating[18-21] have been widely adopted to improve the electrochemical performances of NCA, but these strategies are generally at expense of a loss of capacity. Recently, considerable efforts have been made to synthesis of micro/nanostructured cathode materials with diverse morphologies, aiming to enhance their rate capabilities and cycle lives, for example, $LiCoO_2$ microflakes,[22] $LiFePO_4$ hollow spheres,[23] dumbbell-like $LiNi_{1/3}Co_{1/3}Mn_{1/3}O_2$,[24] and $LiMn_2O_4$ nanorods.[25,26] Among them, one-dimensional (1D) architectures like rod, wire and tube are particularly attractive, since they not only allow both Li^+ ions and electrons to be inserted into 1D architectures synchronously, rendering them ionically and electronically conductive simultaneously, but the large surface-to-volume ratio of the 1D materials also provide efficient electrode-electrolyte contact areas, giving rise to high rate capabilities.[26] To date, however, few attempts have been made to elaborately fabricating NCA with specific structure and morphology. Yang *et al*. recently reported the synthesis of yolk-shell $LiNi_{0.8}Co_{0.15}Al_{0.05}O_2$ spheres by using an ultrasonic atomization method,[27] in which the prepared NCA as cathode material exhibited a high discharge capacity and a good cycle performance. Unfortunately, this yolk-shell NCA only delivered an initial coulombic efficiency less than 85%, whilst suffering from a severe decline in capacity at high discharge rates. In this regard, it is being intensively pursued to develop novel approaches for rational design and facile synthesis of structurally well-defined NCA cathode materials with highly reversible lithium storage properties.

Herein, we report a facile surfactant-free method to prepare 1D $LiNi_{0.8}Co_{0.15}Al_{0.05}O_2$ microrods (denoted as NCA-MRs) using mixed metal oxalate ($MC_2O_4{\cdot}2H_2O$, M= Ni, Co, Al) microrods as precursors obtained *via* a two-step co-precipitation route. The synthetic strategy was illustrated in Fig. 1. First, $CoC_2O_4{\cdot}2H_2O$ microrods were

[a] *Department of Advanced Energy Materials, College of Materials Science and Engineering, Sichuan University, Chengdu 610064, P. R. China. E-mail: hao.wu@scu.edu.cn; y_zhang@scu.edu.cn.*

Electronic Supplementary Information (ESI) available: [Experimental and characterization details; Fig S1-S9 and Table S1-S5]. See DOI: 10.1039/x0xx00000x

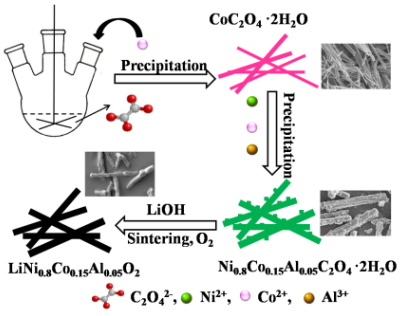

Fig.1 Schematic diagram of preparation processes for NCA-MRs

prepared and chosen as starting materials, not only due to their 1D rod-like structures (Fig. S1 and S2, ESI†), but also because their synthesis can be simply completed by a co-precipitation method without any surfactants involved. We used the as-prepared $CoC_2O_4 \cdot 2H_2O$ crystallite rods as seeds to allow the formation of mixed Ni, Co, and Al oxalates, templated on the initial $CoC_2O_4 \cdot 2H_2O$ rods during the subsequent co-precipitation. The resultant rod-like $MC_2O_4 \cdot 2H_2O$ as precursors were then lithiated to give the final product of 1D $LiNi_{0.8}Co_{0.15}Al_{0.05}O_2$ microrods. For the purpose of comparison, we also synthesized $LiNi_{0.8}Co_{0.15}Al_{0.05}O_2$ microspheres (denoted as NCA-MSs) by using commercial spherical $Ni_{0.8}Co_{0.15}Al_{0.05}(OH)_2$ as precursors to be sintered with LiOH (see the Experimental section in the ESI†).

The crystal phase and composition of the as-prepared NCA-MRs and NCA-MSs as well as their corresponding precursors were first examined using XRD. As shown in Fig. S3 (ESI†), all the diffraction peaks of the $MC_2O_4 \cdot 2H_2O$ precursor for NCA-MRs correspond well to the standard substances including $NiC_2O_4 \cdot 2H_2O$ (JCPDS: 25-0582) and $CoC_2O_4 \cdot 2H_2O$ (JCPDS: 25-0250), while the diffraction peaks of the $Ni_{0.8}Co_{0.15}Al_{0.05}(OH)_2$ precursor for NCA-MSs can be assigned to a solid solution of $Ni(OH)_2$ (JCPDS: 14-0117) and $Co(OH)_2$ (JCPDS: 30-0443). Notably, neither the diffraction peaks of $Al_2(C_2O_4)_3 \cdot xH_2O$ nor that of $Al(OH)_3$ can be observed in their respective XRD patterns, due to their relatively low content. After sintering with LiOH, all the diffraction peaks of NCA-MRs and NCA-MSs can be indexed to typical α-$NaFeO_2$ layered structure with a space group of R-3m, and no impurity peaks were observed, as shown in Fig. S4 (ESI†). Moreover, the strong peak splitting of (006)/(012) and (018)/(110) pairs demonstrates the highly ordered layered hexagonal structure of the two products. The lattice parameters were calculated by the XRD data and listed in the Table S1 (ESI†), in which the parameter *c* is the average metal-metal interslab distance of layer structure, and the lager layer interslab distance is generally associated with fast Li^+ ions insertion/extraction.[28] Clearly, the layer distance of NCA-MRs (*c*=14.1273) is larger than that of NCA-MSs (*c*=14.0822), implying that a better rate performance of NCA-MRs would be obtained. Besides, the larger *c/a* ratio of NCA-MRs suggests that the lattice has the priority to grow along *c* axis, while the value of ratio (4.9344) is more close to that of $LiNiO_2$ (4.935), indicating that NCA-MRs have a lower degree of Li^+/Ni^{2+} mixing and a better layer structure than NCA-MSs.[29] The peak ratio of (003)/(104), an indicator of cation mixing, was also calculated and listed in Table S1 (ESI†), in which in comparison with NCA-MSs, the NCA-MRs shows a relatively larger value of (003)/(104) ratio, indicating its lower cation mixing degree, meaning a smaller concentration of Ni^{2+} ions

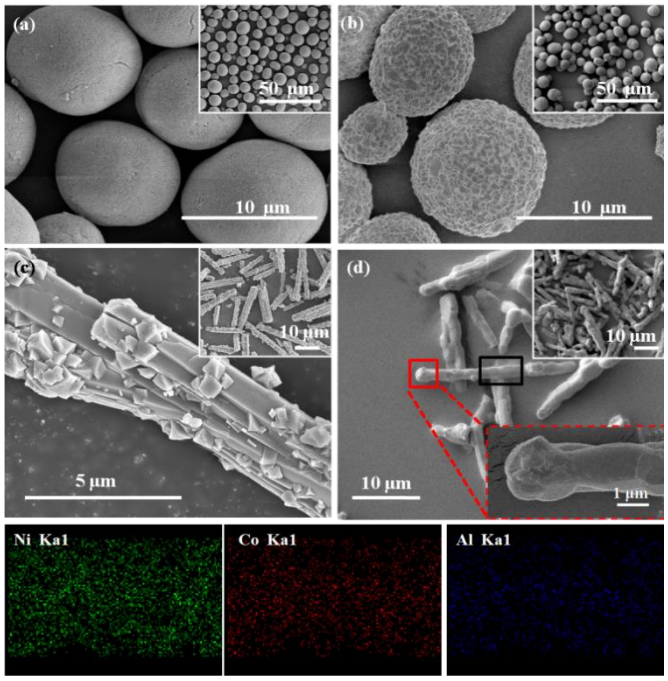

Fig. 2 SEM images of (a) $Ni_{0.8}Co_{0.15}Al_{0.05}(OH)_2$ precursor, (b) NCA-MSs, (c) $MC_2O_4 \cdot 2H_2O$ precursor, and (d) NCA-MRs, insets in above images show the SEM images at low magnification; and EDS dot-mapping of Ni, Co, Al elements of NCA-MRs.

in the Li (3b) interlayer sites. In addition, the *R*-factor of NCA-MRs was estimated to be 0.443 (Table S1, ESI†), which is smaller than that of NCA-MSs (0.469), demonstrating that the NCA-MRs has a better hexagonal structural ordering than NCA-MSs.

The morphology and detailed structure of the as-prepared materials were studied using SEM. As shown in Fig. 2a and b, both $Ni_{0.8}Co_{0.15}Al_{0.05}(OH)_2$ precursor and NCA-MSs exhibit microsized round-shaped morphologies under the SEM observations, which is identical to previous reports.[18,21,30] The inset in Fig. 2c displays a panoramic SEM image of the rod-like $MC_2O_4 \cdot 2H_2O$ precursor, which are generally monodispersed with about 1-2 μm in width and 15-20 μm in length. From a magnified SEM image of a single microrod (Fig. 2c), it can be seen that in comparison with the $CoC_2O_4 \cdot 2H_2O$ microrods (Fig S2, ESI†), each $MC_2O_4 \cdot 2H_2O$ microrod has an uneven surface, on which some irregular particles with sharp edge are adhered, indicating the precipitation of Ni, Co, and Al oxalates on the surface of initial $CoC_2O_4 \cdot 2H_2O$ microrods, confirmed by the EDS dot-mapping spectrum in Fig. S5 (ESI†). Fig. 2d shows the SEM image of the NCA-MRs which still exhibit rod-like morphology with about 1.5 μm in width and 15-20 μm in length, being well inherited from the morphology of the $MC_2O_4 \cdot 2H_2O$ microrod precursor even after sintering with LiOH.

Moreover, the inset in Fig. 2d, a magnified SEM image taken from the red square region, clearly manifests that each microrod has an uninterrupted and compact architecture since there is no obvious void space caused by the aggregation of primary particles observed on the microrod surface. Nitrogen adsorption measurements were further performed on the NCA-MRs and NCA-MSs, by which the BET specific areas of the two products are estimated to be 0.504 and 1.267 m^2/g. This demonstrates that there could be more void spaces or microcracks present in the NCA sphere than the NCA rod.

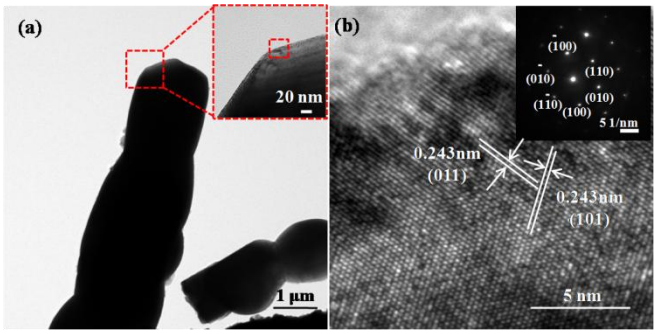

Fig. 3 (a) TEM image of NCA-MRs, the inset shows the magnified region marked by a red square; (b) HRTEM image and SAED pattern from the selected square region in (a).

As known, the Ni-rich cathode materials, commonly prepared by a co-precipitation method are composed of round-shaped secondary particles in which microsized primary particles (grains) are aggregated.[13] However, there are many microcracks between the primary particles, which could act as new reaction sites with electrolytes, leading to formation of solid electrolyte interface (SEI) layers along the active surfaces of primary particles developed by these microcracks. As a result, the transport of electrons and lithium ions through the grain-electrolyte interface would be inhibited, thus diminishing the electrical performance.[31,32] As demonstrated from the SEM images in Fig. 2, the rod-like NCA-MRs has a more compact architecture than the round-shaped NCA-MSs, implying there would be a significant difference in the electrochemical behaviors towards the two products when used as cathode materials for LIBs. EDS dot-mapping for Ni, Co, and Al of the NCA-MRs further reveals that these elements homogeneously distribute in the selected region of the microrods (marked by black rectangle in Fig. 2d). The chemical compositions of the NCA-MRs determined by ICP-AES analysis (Table S2, ESI†) also indicate that the molar ratio of Ni, Co, and Al in these microrods is highly close to the added stoichiometric value of 0.8:0.15:0.05. In addition, XPS was used to determine the surface elements in the NCA-MRs (Fig. S6, ESI†), by which the dominating Ni $2p_{3/2}$ peak appearing at 855.2 eV corresponds well to Ni^{3+} as expected for a typical NCA material,[33] while the Al 2p signal detected within the material surface confirms that Al was successfully co-precipitated with Ni and Co by using oxalic acid as the precipitate reagent.

TEM combined with selected area electron diffraction (SAED) were used to investigate the morphology and structure of the NCA-MRs. As shown in Fig. 3a, the NCA-MRs exhibits a thick and dense rod feature with about 1.5 μm in width, which is in agreement with the SEM observations. Fig. 3b gives the high-resolution TEM (HRTEM) image taken from the red region marked in Fig. 3a, which displays two sets of clear lattice fringes with the same interplanar distance of 0.243 nm, which is consistent with the *d*-spacing of (011) and (101) planes of layered hexagonal phase of $LiNi_{0.8}Co_{0.15}Al_{0.05}O_2$, respectively.[34] In addition, the corresponding SAED pattern (inset in Fig. 3b), showing an array of hexagonal symmetry dots, reveals the single crystalline nature of the NCA microrods.

In view of the unique 1D microrod structure, NCA-MRs might serve as promising cathode materials for LIBs. Hence, the electrochemical measurements were carried out to evaluate the lithium storage performances of the as-prepared products. Fig. 4a shows the typical initial charge-discharge curves of NCA-MRs and NCA-MSs in the voltage range of 2.7-4.3 V at 25 ℃ under a current rate of 0.1C (1C=180 mAh/g). The charge-discharge curves of the two cells are smooth with a monotonous voltage plateau, whereas the NCA-MRs obviously exhibits a longer discharge plateau than NCA-MSs. Accordingly, the initial discharge capacity of the NCA-MRs reaches to about 218 mAh/g, higher than that of the NCA-MSs (195 mAh/g), while their initial coulombic efficiencies are estimated to be 92% and 86%, respectively. Fig. 4b compares the rate performances of the cells evaluated at variable current rates of 0.1-10C for 5 cycles at each current rate. It is clearly discerned that the capacities of both cells decreased as cycling current rate increased (Fig. S7, ESI†), due to the low diffusion rate of the Li^+ ions intercalate/deintercalate electrodes at high rates.[35] Nevertheless, the NCA-MRs can be reversibly cycled at 0.1, 0.2, 0.5, 1, 2, 5 and 10C with stable discharge capacities of 218, 200, 181, 172, 159, 137 and 115 mAh/g, respectively, which is much better than NCA-MSs, especially at high current rate like 5 and 10C (Table S3, ESI†). It should be noticed that when the current rate reversed back to 0.1C after the high rate cycling measurements, a stable high discharge capacity of about 214 mAh/g can be recovered for the NCA-MRs cell. This confirms that the NCA microrods are able to tolerate high rate cycling, which is desirable for high power applications.

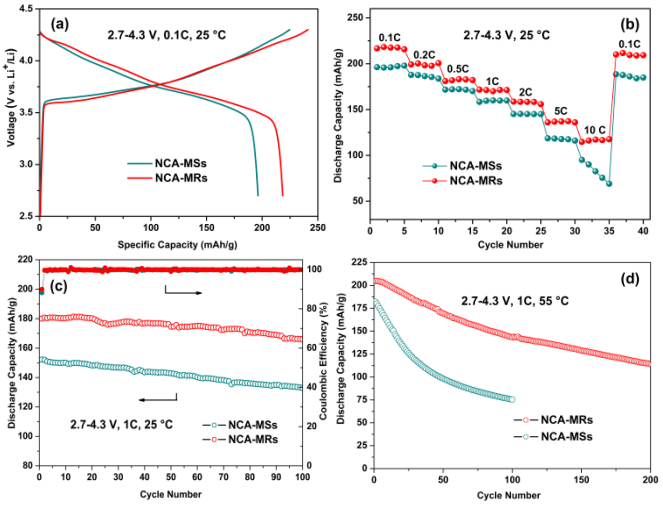

Fig.4 (a) Initial charge and discharge curves of NCA-MSs and NCA-MRs under a current rate of 0.1C; (b) Rate capability under variable current rate; (c and d) Cycling performance at 25 and 55 ℃ under a current rate of 1C. All measurement were conducted in the voltage range of 2.7–4.3 V vs. Li/Li^+.

The cycling performances of NCA-MRs and NCA-MSs at 1C are depicted in Fig. 4c. Clearly, the NCA-MRs exhibits excellent cyclic capacity retention as high as 93% at the end of the 100th cycle, at which a reversible capacity of about 168 mAh/g can still be retained (Fig. S8, ESI†). However, under the identical test conditions, the NCA-MSs displays a relatively faster capacity fading from 152 to 133 mAh/g after 100 cycles, corresponding to the capacity retention of only 87% (Table. S4, ESI†). Electrochemical impedance spectra (EIS) measurements of the cells after 100 cycles were carried out to shed light on the good cycling performance of the NCA-MRs. As can be seen from Fig. S9 (ESI†), the diameter of the semicircle at high

frequencies is much smaller in the plot of NCA-MRs than that of NCA-MSs, indicating the remarkably decreased charge-transfer resistance at the electrode-electrolyte interface, resulted from the merits of 1D rod-like structure of the NCA-MRs. Moreover, the Li^+ ions diffusion coefficient (D_{Li}) is also calculated (Table S5, ESI†), which confirms the faster Li^+ ion diffusion within NCA-MRs than NCA-MSs. These observations indicate that the superior electronic and ionic conductivity of the NCA microrods favours the fast transfer of electron and Li^+ ions in the electrode, thereby enabling NCA-MRs cathode material to manifest much better lithium storage properties than NCA-MSs, in terms of higher discharge capacity, better rate capability and superior cycling stability.

The inferior cycle life of NCA cathode materials at elevated temperature poses a formidable hurdle for their scalable applications. Hence, the cycling stability of NCA-MRs at 55 ℃ was also investigated (Fig. 4d). At 55 ℃, the initial discharge capacities of NCA-MSs and NCA-MRs are 182 and 204 mAh/g, respectively (Table S4, ESI†), which are higher than those obtained at 25 ℃. This phenomenon is attributed to the increased electrochemical activity at higher temperature, which is commonly observed in Ni-based cathode containing a high amount of Ni. At 55 ℃, the NCA-MRs still shows an excellent thermal stability, and it retains 72% of the initial capacity (204 mAh/g) after 100 cycles at the current rate of 1C, whereas the NCA-MSs exhibits an inferior cycle life at this elevated temperature, and it loses its capacity very rapidly as it only deliveries 75 mAh/g (41% retention) after 100 cycles. Furthermore, the NCA-MRs also shows a robust thermal stability in the extended cycle number, as a high reversible capacity of 116 mAh/g (57% retention) is still retained even after total 200 cycles (Table S4, ESI†). Such an impressive electrochemical performance of the NCA microrods could be ascribed to the high structural stability of the single crystalline and uninterrupted 1D microrod architecture with high length/radius aspect ratio, which allows efficient electrode-electrolyte contact, and provides 1D electron transport pathways.

To examine the integrity of the rod-like morphology of NCA-MRs after high-temperature cycling, we carried out post-mortem analyses on the cycled electrodes. Fig. S10a and S10b (ESI†) present the SEM images of the NCA-MSs and NCA-MRs electrodes after the 100th cycle at 55 ℃. Obviously, after high-temperature cycling the NCA-MSs electrode has lost its initial morphology characteristics of microsphere, as there form lots of broken and pulverized particles. On the contrary, the 1D rod-like architecture of the NCA-MRs electrode has been well preserved after cycling, even though the rod surface became pretty rough, which is an indicative of the formed protective SEI films.[36] Additionally, the results from XRD analyses (Fig. S10c, ESI†) also demonstrate that even after long-term charge-discharge cycling, the NCA-MRs electrode still maintained a good layered structure, whereas a significant phase structure transition has occurred in the cycled NCA-MSs electrode, due to the invisible peak splitting between (006) and (102) in its XRD pattern. These facts suggest that the thick and dense microrod structure enables a better tolerance to stress from volume expansion during repeated lithiation/delithiation process, which endows long-term cycling and thermal stability to the as-synthesized NCA microrods.

In summary, we have developed a facile strategy for the synthesis of $LiNi_{0.8}Co_{0.15}Al_{0.05}O_2$ microrods using mixed metal oxalate ($MC_2O_4{\cdot}2H_2O$, M= Ni, Co, Al) microrods as self-sacrificial templates. When evaluated for lithium storage properties, the NCA microrods as cathode materials manifest high specific capacity (~218 mAh/g at 0.1C), good high rate capability (~115 mAh/g at 10C), and superior cycling stability at room and elevated temperature, as compared with commercial NCA microspheres. The excellent lithium storage performances of the synthesized NCA microrods might be attributed to their well-defined 1D rod-like architecture with high structural stability. All the results suggest the promising potential of the NCA microrods as advanced cathode materials for LIB applications.

The authors acknowledge the financial supports from National Basic Research Program of China (973 program no. 2013CB934700), A Foundation for the Author of National Excellent Doctor Dissertation of P. R. China (no. FANEDD201435), and the Sichuan Province Science and Technology Support Program (no. 2014GZ0093).

Notes and references

1 J. B. Goodenough, *Energy Enviro. Sci.*, 2013, **7**, 14-18.
2 J. Chen, *Materials*, 2013, **6**, 156-183.
3 T. Kim, J. Park, S. K. Chang, S. Choi, J. H. Ryu and H. Song, *Adv. Energy Mater.*, 2012, **2**, 860-872.
4 M. Jo, M. Noh, P. Oh, Y. Kim and J. Cho, *Adv. Energy Mater.*, 2014, **4**, 1301583-1301590.
5 H. Chen, J. A. Dawson and J. H. Harding, *J. Mater. Chem. A*, 2014, **2**, 7988-7996.
6 S. Hwang, W. Chang, S. M. Kim, D. Su, D. H. Kim, J. Y. Lee, K. Y. Chung and E. A. Stach, *Chem. Mater.*, 2014, **26**, 1084-1092.
7 C. Fu, G. Li, D. Luo, Q. Li, J. Fan and L. Li, *ACS Applied Mater. Inter.*, 2014, **6**, 15822-15831.
8 C. H. Chen, J. Liu, M. E. Stoll, G. Henriksen, D. R. Vissers and K. Amine, *J. Power Sources*, 2004, **128**, 278-285.
9 G. Q. Tan, F. Wu, J. Lu, R. J. Chen, L. LiandK. Amine, *Nanoscale*, 2014, **6**, 10611-10622.
10 C. Delmas and I. Saadoune, *Solid State Ionics*, 1992, **53-56**, 370-375.
11 T. Ohzuku, T. Yanagawa, M. Kouguchi and A. Ued, *J. Power Sources*, 1997, **68**, 131-134.
12 S. Madhavi, G. V. Subba Rao, B. V. R. Chowdari and S. F. Y. Li, *J. Power Sources*, 2001, **93**, 156-162.
13 K. Kleiner, D. Dixon, P. Jakes, J. Melke, M. Yavuz, C. Roth, K. Nikolowski, V. Liebau and H. Ehrenberg, *J. Power Sources*, 2015, **273**, 70-82.
14 S. M. Bak, K. W. Nam, W. Chang, X. Q. Yu, E. Y. Hu, S. Hwang, E. A. Stach, K. B. Kim, K. Y. Chung and X. Q. Yang, *Chem. Mater.*, 2013, **25**, 337-351.
15 T. H. Tran, S. Harmand, B. Desmet and F. Pailhoux, *J. Electrochem. Soc.*, 2013, **160**, A775-A780.
16 T. Sasaki, V. Godbole, Y. Takeuchi, Y. Ukyo and P. Nova K, *J. Electrochem. Soc.*, 2011, **158**, A1214-A1219.
17 A. H. Tavakoli, H. Kondo, Y. Ukyo and A. Navrotsky, *J. Electrochem. Soc.*, 2012, **160**, A302-A305.
18 S. Lee, C. S. Yoon, K. Amine and Y. Sun, *J. Power Sources*, 2013, **234**, 201-207.
19 D. N. Qian, B. Xu, H. M. Cho, T. Hatsukade, K. J. Carroll and Y. S. Meng, *Chem. Mater.*, 2012, **24**, 2744-2751.
20 D. Lee, B. Scrosati and Y. Sun, *J. Power Sources*, 2011, **196**, 7742-7746.
21 S. N. Lim, W. Ahn, S. Yeon and S. B. Park, *Electrochim. Acta*, 2014, **136**, 1-9.
22 T. Wei, R. Zeng, Y. Sun, Y. Huang and K. Huang, *Chem. Commun.*, 2014, **50**, 1962-1964.

23 M. Lee, J. Kim and H. Song, *Chem. Commun.*, 2010, **46**, 6795-6797.
24 W. Ryu, S. Lim, W. Kim and H. Kwon, *J. Power Sources*, 2014, **257**, 186-191.
25 D. K. Kim, P. Muralidharan, H. Lee, R. Ruffo, Y. Yang, P. Chan, R. A. Huggins and Y. Cui, *Nano Lett.*, 2008, **8**, 3948-3952.
26 X. L. Zhang, F. Y. Cheng and J. Yang, *Nano Lett.*, 2013, **13**, 2282-2825.
27 H. Yang, P. Liu, Q. Chen, X. Liu, Y. Lu, S. Xie, L. Ni, X. Wu, M. Peng, Y. Chen, Y. Tang and Y. Chen, *RSC Advances*, 2014, **4**, 35522-35527.
28 Y. Sun, B. Lee, H. Noh, H. Wu, S. Myung and K. Amine, *J. Mater. Chem.*, 2011, **21**, 10108-10112.
29 C. Lu, H. Wu, Y. Zhang, H. Liu, B. J. Chen, N. T. Wu and S. Wang, *J. Power Sources*, 2014, **267**, 682-691.
30 H. Y. Tran, G. Greco, C. Täubert, M. Wohlfahrt-Mehrens, W. Haselrieder and A. Kwade, *J. Power Sources*, 2012, **210**, 276-285.
31 H. Wang, Y. Jang, B. Huang, D. R. Sadoway and Y. M. Chiang, *J. Electrochem. Soc.*, 1999, **146**, 473-480.
32 S. Watanabe, M. Kinoshita, T. Hosokawa, K. Morigaki and K. Nakura, *J. Power Sources*, 2014, **258**, 210-217.
33 H. Liu, Y. Yang and J. Zhang, *J. Power Sources*, 2006, **162**, 644-650.
34 F. Fu, G. Xu, Q. Wang, Y. Deng, X. Li, J. Li, L. Huang and S. Sun, *J. Mater. Chem. A*, 2013, **1**, 3860-3864.
35 Z. Wang, S. Huang, B. Chen, H. Wu and Y. Zhang, *J. Mater. Chem. A*, 2014, **2**, 19983-19987.
36 P. Verma, P. Maire and P. Novak, *Electrochim. Acta*, 2010, **55**, 6332-6341.